Ceramics International xxx (xxxx) xxx

Contents lists available at ScienceDirect

Ceramics International

journal homepage: www.elsevier.com/locate/ceramint

Dual-emitting phosphor-glass composites by the melt-quenching method for high-quality laser lighting

Wenting Ding [a], Zeliang Zhang [a], Xin Hou [a], Yang Mei [a], Deng Long [b], Leiying Ying [a], Miao Lu [b], Baoping Zhang [a,*]

[a] Department of Microelectronics and Integrated Circuits, Laboratory of Micro/Nano-Optoelectronics, School of Electronic Science and Engineering, Xiamen University, Xiamen, 361005, PR China

[b] Pen-Tung Sah Research Institute of Micro-Nano Science & Technology, Xiamen University, Xiamen, 361005, PR China

ARTICLE INFO

Keywords:
Phosphor-glass composites
Melt-quenching
Dual-layer structure
Laser lighting

ABSTRACT

The development of color converters with excellent low-cost comprehensive indicators is of great significance in promoting the rapid development of laser lighting technology. In this work, low-cost phosphor-glass composites (PGC) including green-emitting $Lu_3Al_5O_{12}:Ce^{3+}$ (LuAG) and red-emitting $CaAlSiN_3:Eu^{2+}$ (CASN) phosphors were successfully prepared by the melt quenching method. Moreover, the two phosphor layers were uniquely designed to be separated in a stable dual-layer structure supported by the matrix glass. This double layer structure can effectively reduce the reabsorption in traditional mixed multi-color phosphors. The main emission of the PGC-Green exhibited high internal and external quantum efficiencies of 95% and 68.8%, respectively. Meanwhile, the PGC-Red can still achieve the purpose of supplementing red emission, which is conducive to obtaining a higher color rendering index (CRI). Furthermore, the content of the LuAG phosphor and the thickness of the PGC layer were adjusted to reach a balance between efficiency and color. The optimized PGC has a luminous flux of 507 lm at a laser excitation power density of 2.66 W mm^{-2} with maximum luminous efficiency of 190 lm W^{-1}. A stable correlated color temperature of 5600 ± 300 K with a high CRI of 84 was achieved, similar to the sunlight-color profile. In addition, the luminescence of PGC is only reduced by less than 10% at 458 K, showing excellent thermal stability. We believe that this work provides a novel design of high-performance PGC color converters coupled with traditional glass manufacturing processes.

1. Introduction

Light-emitting diodes (LEDs) have many advantages such as high efficiency, long life, small size, and being environmentally friendly [1–3]. They are widely used in lighting, display, and communication [4]. White light is one of the most widely used spectrum of solid-state lighting [5,6]. The implementation of commercial white LEDs through the combination of GaN/InGaN LED chips and color converters is affected by the "efficiency degradation" of the LED chips at high input current density [7,8]. Achieving stable highly-efficient white LEDs working at high power is difficult. In contrast, a laser diode (LD) is effective in avoiding sudden dropping in efficiency and can maintain a stable high efficiency at high power densities with additional advantages of fast response, high brightness, and long irradiation distances [9–11]. Therefore, the development of white light based on a color converter driven by blue LD has attracted the attention of many researchers [12–14].

Traditional color converters made of yellow $Y_3Al_5O_{12}$: Ce^{3+} (YAG) phosphors wrapped in silica gel or organic resin have been criticized for their poor irradiation reliability and thermal stability with the local high temperatures caused by heat build-up under high-power lasers [10,15]. Currently, most published reports focus on color converters for all-inorganic materials, including transparent ceramic phosphors, single-crystal phosphors, and phosphor-glass composites (PGCs) [16,17]. Among them, transparent ceramic phosphors and single-crystal fluorescents have offered excellent optical and thermal properties, although their preparation is complex and costly [18–20]. Their yield is strictly limited by the availability of raw materials and preparation conditions. Within the color converters described above, PGCs, including Phosphor in Glass (PiG) and phosphor-glass composite film (PGF), meet the potential conditions for commercial production due to their low cost, simple preparation process, and diverse phosphor

* Corresponding author.
E-mail address: bzhang@xmu.edu.cn (B. Zhang).

https://doi.org/10.1016/j.ceramint.2022.08.047
Received 11 June 2022; Received in revised form 28 July 2022; Accepted 5 August 2022
Available online 17 August 2022

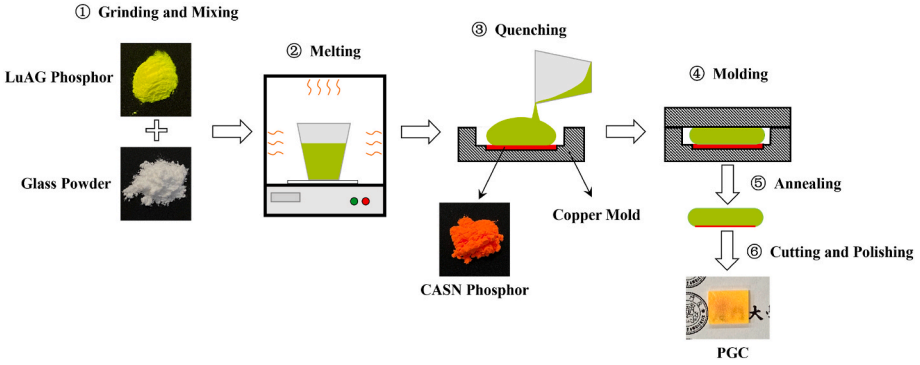

Fig. 1. Schematic of the fabrication process of the PGC.

combinations [21]. Wei et al. created YAG PGFs with sapphire substrates and obtained the luminous flux (LF) of 1709 lm and the luminous efficiency (LE) of 211 lm W^{-1} under the excitation by a 10.3 W mm^{-2} blue laser [22]. Yang et al. successfully prepared YAG PiG by designing the glass composition of Na_2O–CaO–B_2O_3–SiO_2 and achieved a surprising LE of 239.9 lm W^{-1} [23]. Wang et al. carefully assembled the $Lu_3Al_5O_{12}$: Ce^{3+} (LuAG) PiG achieving an increased conversion efficiency of 56.3% from blue to green light with the LE of 225 lm W^{-1} [24]. The preparation of $Y_3Al_{3.5}Ga_{1.5}O_{12}$: Ce^{3+} PiG was optimized by Zhang et al. to achieve the LF of 555.6 lm with an LE of 254.5 lm W^{-1} as the laser density was increased to 2.78 W mm^{-2} [25]. However, these results are mainly focused on high LFs and LEs. Meanwhile, due to the emission characteristics of Ce-doped garnet phosphors, it still lacks effective red emission for producing white light [26,27]. Thus, it is difficult to achieve high-quality white light with high color rendering index (CRI) [28]. To overcome this problem, Liu et al. reported a LuAG/$CaAlSiN_3$:Eu^{2+} (CASN) PGF with a LE of 153 lm W^{-1} and a CRI of 88.6 under the excitation of a 455 nm blue laser [29]. Zhang et al. prepared LuAG/-CASN PiG with a CRI of up to 95 and a LE of 216.79 lm W^{-1} with good heat dissipation [30]. Huang et al. laminated patterned CASN PGF on the LuAG PGF-on-sapphire to obtain a PGF plate with LF of 1408 lm, LE of 74 lm W^{-1}, and CRI of 82 [31]. However, most of the existing multicolored PGC used a low-temperature co-sintering method, which suffered from the processing difficulties, such as porous structure and cracking, uneven distribution of the multicolored phosphors, easy to agglomerate in the glass matrix reabsorption, and low luminescence efficiency [32–34]. At the same time, the corrosion strength of matrix glass on different types of phosphors is not uniform, and the glass melt is prone to interfacial reaction with phosphors, such as CASN, at high temperatures that greatly limits the application of glass components [35, 36].

In this work, based on the TeO_2–B_2O_3–ZnO–Na_2O–Al_2O_3 glass system, PGC containing LuAG/CASN phosphor was successfully prepared by the melt-quenching technique. Due to the physically isolated green and red phosphor layers, PGC has a stable dual-layer structure that effectively mitigates the reabsorption effect [30]. The samples were produced by a simple preparation method at a low melting temperature, which is conducive to reducing costs in mass production. The

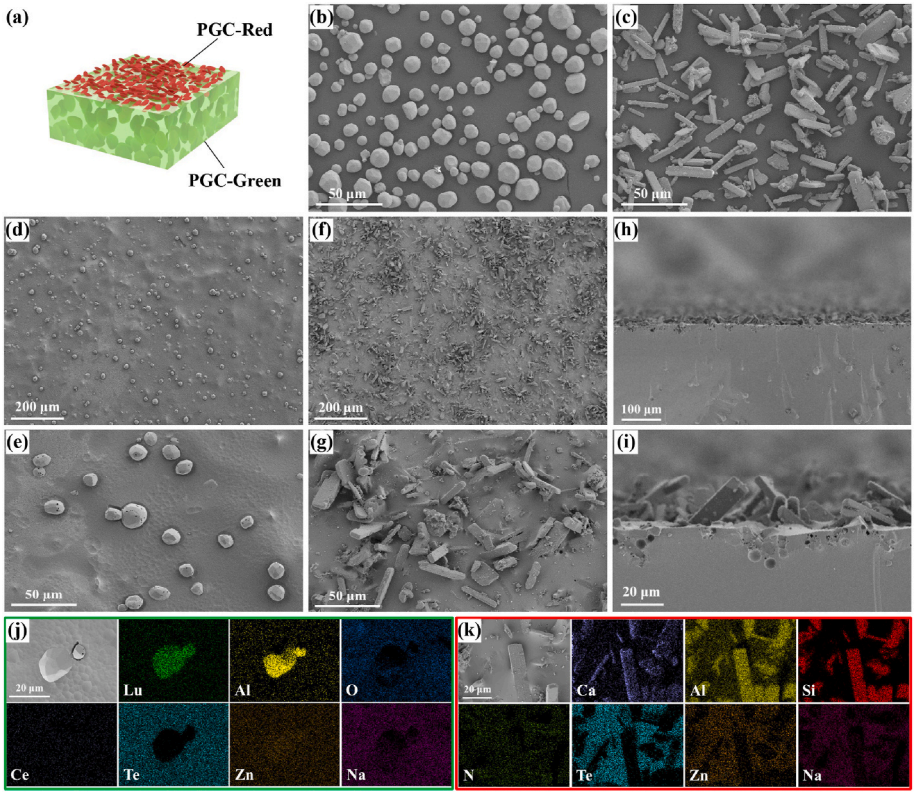

Fig. 2. (a) Schematic diagram of the PGC structure. Morphology characteristics of the (b) LuAG and (c) CASN phosphor. (d) SEM image and (e) high magnification image of the PGC-Green. (f) SEM image and (g) high magnification image of the PGC-Red. (h) Cross-sectional view and (i) high magnification image of the PGC. EDS mapping of the (j) PGC-Green and (k) PGC-Red. (For interpretation of the references to color in this figure legend, the reader is referred to the Web version of this article.)

luminescence and thermal stabilities of the synthesized double layer PGC were characterized. Most importantly, the optimized PGC achieved a high-quality white light output driven by a blue LD with an LE of up to 190 lm W^{-1} and a correlated color temperature (CCT) of about 5600 K, and a CRI of 84, confirming the commercial potential of this color converter in laser lighting.

2. Experimental

2.1. Materials and synthesis

Appropriate amounts of raw materials were weighted based on the composition of $45TeO_2$–$20B_2O_3$–$16ZnO$–$12Na_2O$–$7Al_2O_3$ (mol%). Molar ratio of TeO_2 (99.9%, Adamads), H_3BO_3 (99.9%, Macklin), ZnO (99.9%, Aladdin), Na_2CO_3 (99.9%, Macklin), and Al_2O_3 (98%, Aladdin) were well mixed before loaded into a crucible. The sample was heated and melted in a muffle furnace at 850 °C for 1h. The molten glass liquid is water quenched and then thoroughly ground to obtain fine glass powder which was filtered through a 200 mesh sieve. Glass powder was mixed with a certain mass fraction (8%, 10%, 12%, 14%, and 16%) of LuAG phosphor (Shenzhen looking long technology Co., LTD). The sample was heated to 680 °C in a corundum crucible and kept in a warmer for 0.5 h. At the same time, the bottom groove of a copper mold (groove volume is about 15.71 cm^3) was filled with 0.18 g CASN phosphor powder (Shenzhen looking long technology Co., LTD) with a flattened phosphor surface. The copper mold was heated to 200 °C. After the glass/LuAG mixture was melted, it was quickly poured into the copper mold over the CASN and pressed with a copper cover. After cooling to room temperature, the solids were removed from the mold, annealed at 300 °C for 3 h, and the PGC samples of different thicknesses (0.8, 1.0, 1.2, and 1.4 mm) were obtained after cutting and polishing. The above experiments were completed in an air environment, and the process is shown in Fig. 1.

2.2. Characterization

The crystalline phases in the samples were identified with the use of a powder X-ray diffractometer (XRD, XRD-7000, Shimadzu) supplied by Cu-Kα irradiation source. The microstructures were analyzed using a scanning electron microscope (SEM, SUPRA55 SAPPHIRE, Zeiss) equipped with an energy dispersive spectrometer (EDS) for elementary analysis. Optical transmittance curves of PGCs were conducted from 200 to 800 nm by a UV-VIS spectrophotometer (UV-2550, Shimadzu). The photoluminescence excitation (PLE) and photoluminescence (PL) spectra were examined by a steady state and transient fluorescence spectrometer (FLS1000, Edinburgh) equipped with a 450 W Xenon lamp as the lighting source. The internal and external quantum efficiency (IQE and EQE) of the PGC were tested by the FLS1000 instrument with an integrating sphere accessory (N-M01, Edinburgh). The temperature-dependent PL spectra were collected using a liquid Nitrogen cryostat (Optistat DN, Oxford) attached to the FLS1000. The LF, LE, CCT, CRI, and electroluminescent (EL) spectra of PGCs driven by a 450 nm LD (3 W, Nichia) were recorded using an integrating sphere of 30 cm diameter connected to a photodetector (HAAS-2000, Everfine). The optical power of the blue LD by adjusting to a nearly circular spot (area of 1.098 mm^2) was measured with a laser power meter (PD300, Ophir).

3. Results and discussion

Fig. 2a is a schematic diagram of the PGC structure, named after PGC-Green and PGC-Red to distinguish the components. Fig. 2b-c shows the morphology of the LuAG and CASN phosphors. The LuAG grains are spherical with a small number of sharp surfaces. The average particle size of LuAG is 11 μm. The CASN crystals are rod-shaped with smooth surfaces, and the average particle size is 22 μm (see Fig. S1). SEM images of PGC-Green are shown in Fig. 2d-e. The corresponding LuAG spherical

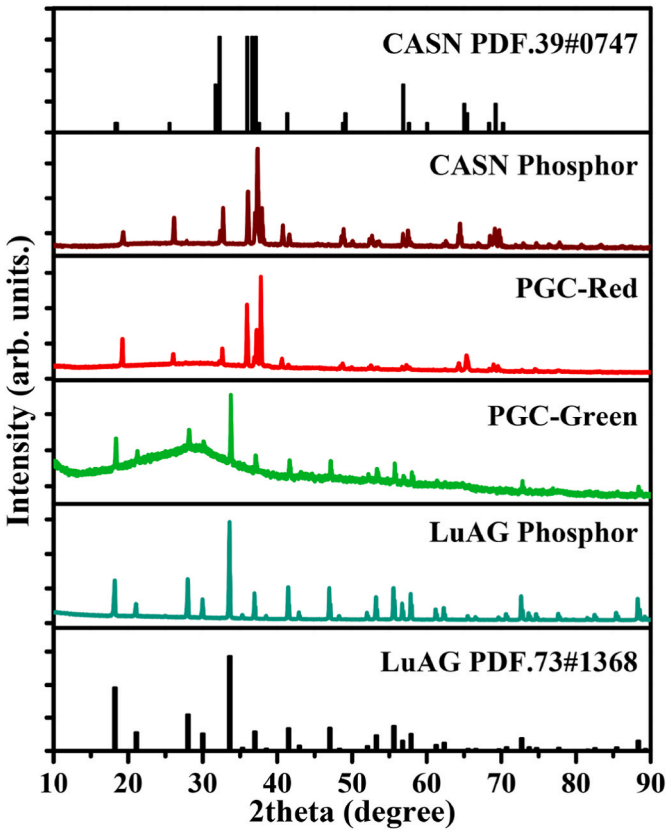

Fig. 3. XRD patterns of the LuAG/CASN phosphor and PGC (divided into PGC-Green and PGC-Red). (For interpretation of the references to color in this figure legend, the reader is referred to the Web version of this article.)

grains were evenly distributed in the matrix glass without significant changing in the particle size. In contrast, the SEM images of PGC-Red show that the rod-like particles of CASN were disordered and densely distributed on the surface of the matrix glass, which is influenced by the bonding process, as shown in Fig. 2f-g. The cross-sectional SEM images in Fig. 2h-i shows that, for the semi-upright orientation of the rod-like CASN, the ends of most of the particles were wrapped by matrix glass to form a stable layer. Fig. 2j-k shows the EDS mappings of the PGC-Green and PGC-Red. The element composition in the PGC-Green region includes Lu, Al, O, Ce, Te, Zn and Na, where Lu, Al and Ce elements are from the LuAG particles, and Te, Zn and Na elements are from the matrix glass. Similarly, the elements displayed in the PGC-Red region were Ca, Al, Si, N, Te, Zn, Na, etc., corresponding to the CASN particles and the matrix glass. This demonstrates that a unique double layer structure PGC was formed by dispersing the LuAG phosphor in the glass matrix and bonding a CASN phosphor film on the surface.

The phase structure of the PGC is characterized by XRD analysis shown in Fig. 3. The presence of intact LuAG is confirmed with the diffraction peaks assigned based on the standard (LuAG PDF. 73#1368) without other peaks, except for some very broad bands from the glass [37]. In contrast, from the XRD data of PGC-Red, the main sharp diffraction peaks from the CASN phosphor were accompanied by some additional weak peaks. Hence, the tellurium component in the matrix glass has caused corrosion and decomposition of the CASN crystals. However, the small contact area and the nature of the separated heterogeneous layers have limited the decomposition only to the surface in contact with the glass matrix, while most of the CASN particles were intact, consistent with the morphological analysis in Fig. 2.

The recorded PGC (divided into PGC-Green and PGC-Red) PLE and PL spectra are shown in Fig. 4a, corresponding to the LuAG and CASN phosphors, respectively. The PGC-Green has identical excitation peaks

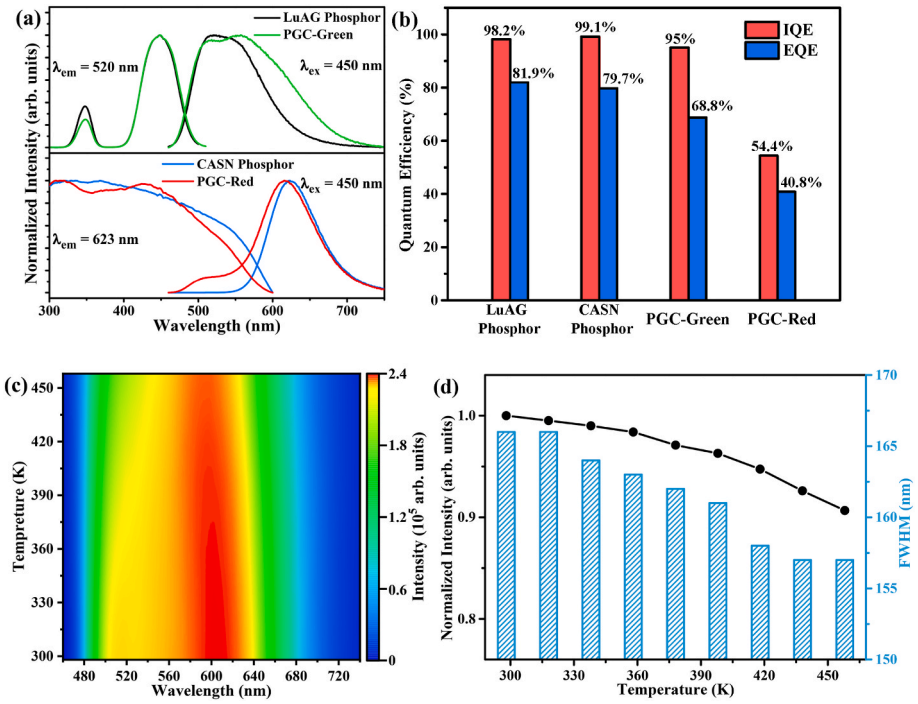

Fig. 4. (a) Normalized PLE and PL spectra, (b) IQE and EQE of the LuAG/CASN phosphor and PGC (divided into PGC-Green and PGC-Red). (c) Temperature-dependent PL spectra, (d) the corresponding normalized PL intensity and FWHM of the PGC with temperature ranging from 298 to 458 K. (For interpretation of the references to color in this figure legend, the reader is referred to the Web version of this article.)

as the LuAG phosphor at 350 and 450 nm due to the Ce^{3+} excitations from the 4f ground state to the $5d_2$ and $5d_1$ excited states. However, the excitation peak at 350 nm is weaker in the PGC-Green than in the LuAG phosphors due to the effect of short-wavelength absorption by the matrix glass. Under the 450 nm excitation, the broadband emission from the LuAG phosphors at 520 nm corresponds to the Ce^{3+} $5d_1 \rightarrow$ 4f relaxation. However, with the same wide emission peak, the emission at 557 nm from the PGC-Green was significantly enhanced. The corresponding half-peak width was increased from 102 nm to 144 nm. Since both LuAG and CASN phosphors exhibited strong absorption at 450 nm, while the matrix glass is highly transparent at 450 nm, some excitation light could be absorbed by the CASN layer. Thus, the emission from the CASN component could also contribute to the total emission. Meanwhile, the emission spectrum from the PGC-Red component is very similar to that from the CASN phosphors, which is originated from the Eu^{2+} $4f_65d \rightarrow 4f_7$ transition [38]. Due to the mitigated self-absorption effect, there is a slight blue shift (from 623 nm to 616 nm) of this emission in addition to a weak broadband emission in the range of 480–550 nm [39]. The IQE and EQE values of the PGC-Green were as high as 95 and 68.8%, respectively, compared to the LuAG phosphors, as presented in Fig. 4b. This is mainly because the large spatial distance between the two luminous centers effectively reduced the photon reabsorption [31]. The IQE and EQE values of the PGC-Red were reduced to 54.4 and 40.8%, respectively. The SEM and XRD results suggest that the matrix glass reacted with CASN grains at high temperatures, which is responsible for the cause of luminescence decrease. Nevertheless, this phenomenon is only limited to the interface, and the intact grains can still provide the expected red emission. The temperature dependent PL spectra were collected and they are shown in Fig. 4c to evaluate the critical thermal stability of the PGC. The luminous intensity of the PGC decreased monotonically as the temperature increased, which is attributed to the occurrence of thermal quenching (the ground state returns to the excited state through non-radiative transitions) [40]. The green and red emission peaks from the PGC were red-shift (from 517 to 529 nm) and blue-shift (from 613 to 598 nm), respectively. The detailed data are shown in Fig. S2. As the temperature rises, the redshift of the green emission peak is due to the increase in the Stokes shift, while the blue shift of the red emission is affected by the heat-activated phonon-assisted tunneling effect [30]. The full width at half maximum (FWHM) of the emission peak was also affected by the temperature, as shown in Fig. 4d. When the temperature was increased to 458 K, 90% of the original emission intensity was maintained from the PGC. Such excellent thermal stability suggests that the double layer PGC is qualified as a laser-driven color converter.

With the excellent optical and thermal performance of the PGC composite, an optical path system is designed for illumination measurement, as shown in Fig. 5a. Since PGC-Red showed an extensive absorption of blue-green light, as presented in Fig. 4a, the excitation blue laser was shined from the PGC-Green side in a transmission mode to achieve the best excitation effect. The actual configuration and

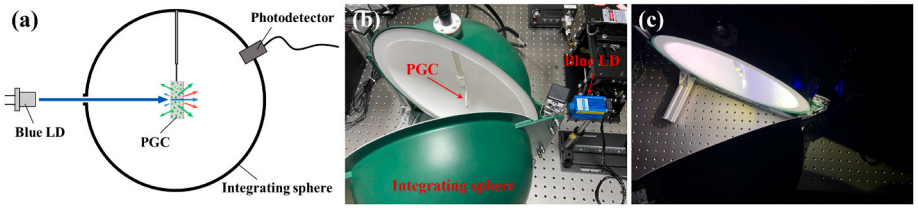

Fig. 5. (a) Schematic diagram of the measurement for laser-driven PGC in transmission mode; photos of the (b) actual configuration and (c) working.

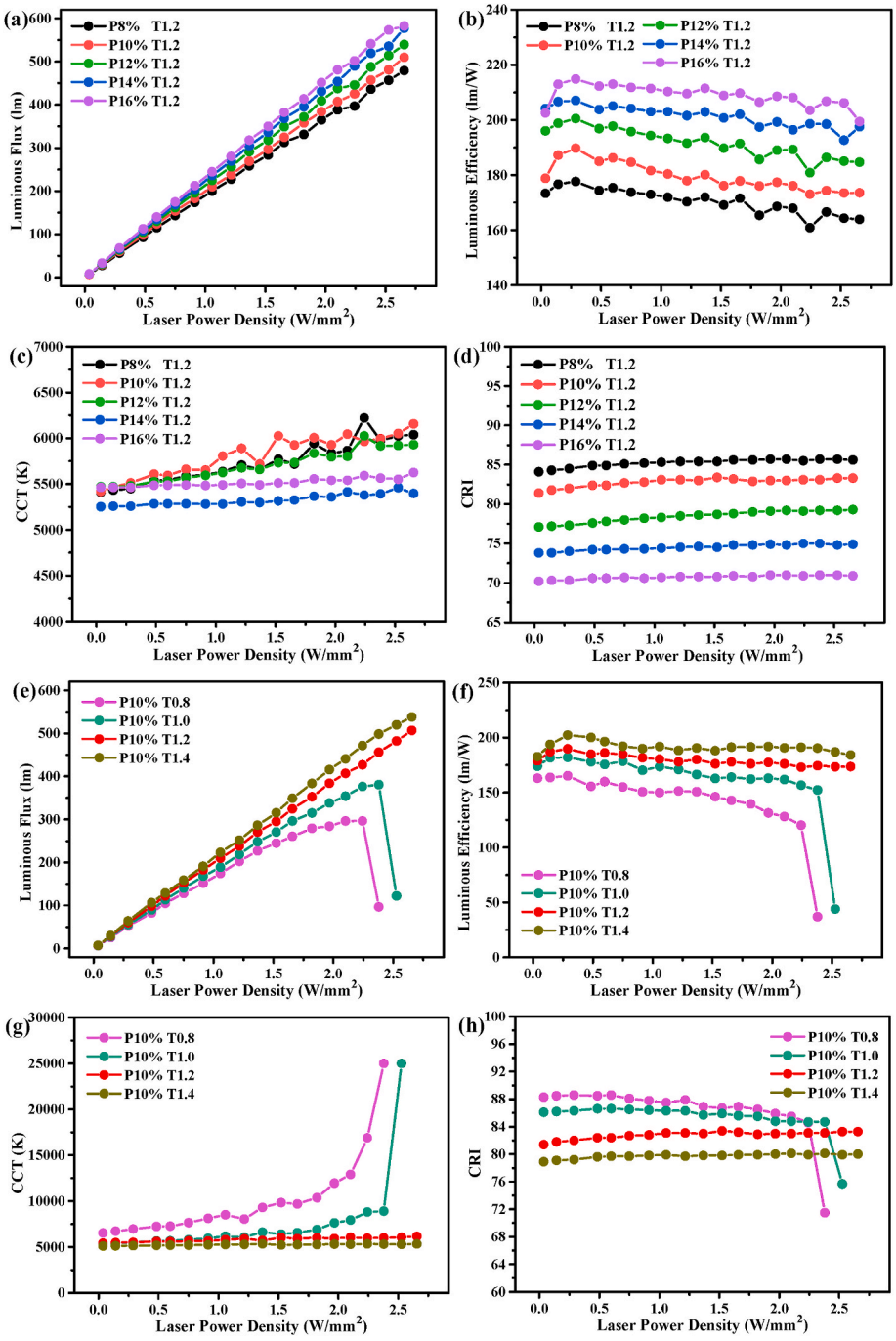

Fig. 6. LF, LE, CCT and CRI of PGCs with different LuAG phosphor contents (a–d) and thicknesses (e–h).

luminescence are shown in Fig. 5b-c.

The samples with different LuAG phosphor concentrations and PGC thicknesses were irradiated by the blue LD. The laser power density was gradually increased to evaluate its potential performance. In Fig. 6a-b, the LF of PGC increases linearly as the laser power density increases. Even at the maximum laser power density of 2.66 W mm^{-2}, the luminescence saturation was still not observed. The corresponding LE was also increased initially. However, after reaching the peak near 0.29 W mm^{-2}, LE showed a stable and slow downward trend due to the phosphor's thermal quenching effect. Meanwhile, the increase in LuAG phosphor content benefits the LF and LE of the PGC. With 16% LuAG concentration, an extremely high LF of 583 lm and a maximum LE of 215 lm W^{-1} were achieved. Meanwhile, from Fig. 6c, the CCT and CRI values of the PGC also increased with the increase of the laser power density. The increase in LuAG phosphor content is conducive to stabilizing the CCT fluctuations, resulting in a more stable white light output. However, the corresponding CRI was negatively correlated with the LuAG concentration with the highest CRI of 85 obtained at the lowest PGC concentration. Since a very low LE reduces the application value of PGC, an appropriate to achieve a balanced CRI and LE. Hence, the LuAG phosphor content was fixed to 10% to test the effects of thickness, as shown in Fig. 6e–h.

The LF and LE of PGC increased with the increase of thickness. At laser power densities of 2.24 W mm^{-2} and 2.38 W mm^{-2}, the P10% T0.8 and P10% T1.0 samples reached luminescence saturation followed by quenching. The sample showed signs of melting with the red layer scorched black, which is attributed to its low thickness. Since the green phosphor layer did not absorb enough blue light, high-density laser

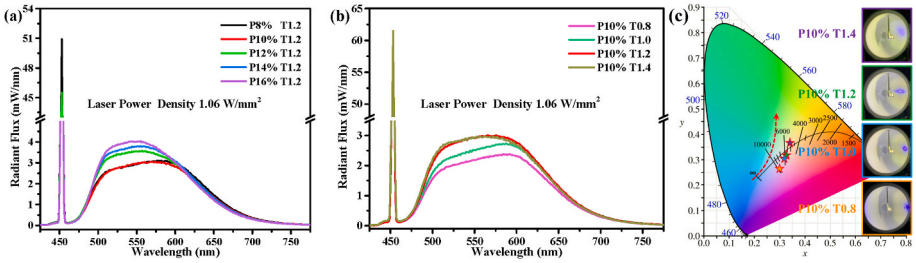

Fig. 7. The EL spectra of PGCs with different (a) LuAG phosphor concentrations and (b) thicknesses under the same laser power density; (c) CIE color coordinates of PGCs with different thicknesses, the inset of (c) shows actual luminescence photos. (For interpretation of the references to color in this figure legend, the reader is referred to the Web version of this article.)

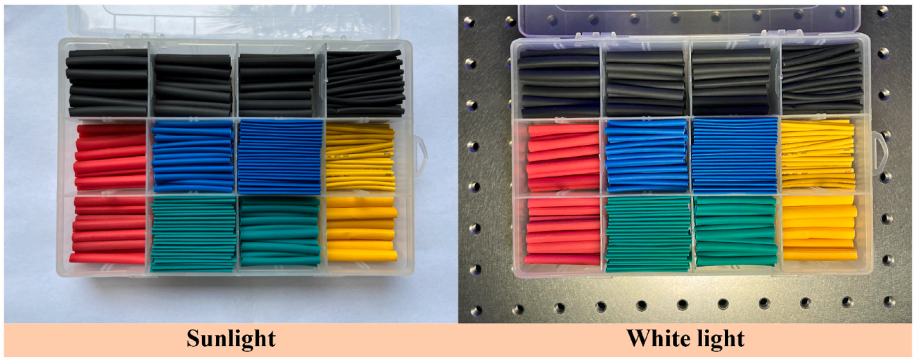

Fig. 8. Color performance in sunlight and white light obtained by laser pumping PGC of this work. (For interpretation of the references to color in this figure legend, the reader is referred to the Web version of this article.)

irradiation on the red phosphor layer was above its absorption limit, resulting in rapid heat accumulation without sufficient dissipation. This sharp increase in the temperature caused the PGC damage [24]. The overall maximum LF and LE were obtained from the P10% T1.4 sample with 538 lm and 202 lm W^{-1}. Conversely, Fig. 6g-h demonstrated a significant decrease in the CCT and CRI values with the increase of the PGC thickness. Among them, the CCT values of P10% T1.4 and P10% T1.2 samples were 5200 ± 100 and 5600 ± 300 K, respectively, with the corresponding CRI values of 80 and 84. These data suggest that an increase in LuAG phosphor content and thickness will improve the LF and LE of PGC at the expense of CCT and CRI.

Fig. 7a-b shows the EL signals as a function of LuAG phosphor concentration and the thickness of PGC at a fixed laser power density. Even though the PGC transmittance is low (see Fig. S3), the red fluorescent layer can still be effectively excited by the penetrated laser light, bringing its emission center closer to 600 nm. As the LuAG phosphor concentration and thickness gradually increase, the green emission is enhanced, resulting in the total emission peak of the PGC shifting to short wavelengths [29]. The color coordinates of the mixed light in the integrating sphere will penetrate deep into the yellow-green region, as shown in Fig. S4 and Fig. 7c. Based on the above results, we believe that the P10% T1.2 sample has a balance of LE and CRI, which aligns with the characteristics of an excellent laser-driven color converter.

Finally, the white light obtained by the laser pumped PGC is compared with the color performance of daylight, as shown in Fig. 8. It is satisfactory that the produced white light nearly matched the red, green, and blue components of the sunlight with excellently balanced yellow color, which satisfied the need for a single red layer to supplement red light. This laser-driven LuAG/CASN PGC offered an almost ideal white light with excellent LF, LE, CCT (5000–5500K), and CRI parameters (summarized in Table S1).

4. Conclusion

In summary, we successfully prepared a LuAG/CASN PGC structure by the melt-quenching method based on a telluride glass matrix. According to the morphological and structural analysis, this method not only successfully maintains the crystal structure of the LuAG phosphor, but also avoids the excessive corrosion and decomposition of the CASN phosphors in contact with the matrix glass. A stable bilayer structure containing both LuAG and CASN phosphors is produced with the controlled LuAG concentration and film thickness. The corresponding PGC-Green shows excellent green emission with high IQE and EQE of 95% and 68.8%, respectively. Although the IQE and EQE parameters of PGC-Red are reduced to 54.4 and 40.8%, respectively, it can still achieve the purpose of supplementing the red color. Besides, PGC still retains more than 90% of the original emission intensity at 458 K. The excellent luminescence and thermal stability guarantee a stable light output under the blue laser illumination. The optical and color properties of the structure were optimized by adjusting the content and thickness of the LuAG phosphor. The resulting white light LF is up to 507 lm (450 nm laser power density of 2.66 W mm^{-2}) and a maximum LE of 190 lm W^{-1}, while its excellent color performance is represented by a stable CCT of 5600 ± 300 K and a high CRI of 84. The results strongly demonstrate the commercial potential of the PGC as a dual-emitting color converter in the field of high-quality laser lighting. Moreover, this work provides an innovative idea for bringing traditional glass manufacturing processes to synthesizing functional materials.

Declaration of competing interest

The authors declare that they have no known competing financial interests or personal relationships that could have appeared to influence the work reported in this paper.

Acknowledgements

This work was supported by the National Key Research and Development Program of China (Nos. 2017YFE0131500), the National Natural Science Foundation of China (Nos. 62104204 and U21A20493).

Appendix A. Supplementary data

Supplementary data to this article can be found online at https://doi.org/10.1016/j.ceramint.2022.08.047.

References

[1] Y. Zhou, W. Zhuang, Y. Hu, R. Liu, H. Xu, M. Chen, Y. Liu, Y. Li, Y. Zheng, G. Chen, Cyan-green phosphor $(Lu_2M)(Al_4Si)O_{12}:Ce^{3+}$ for high-quality LED lamp: tunable photoluminescence properties and enhanced thermal stability, Inorg. Chem. 58 (2) (2019) 1492–1500, https://doi.org/10.1021/acs.inorgchem.8b03017.

[2] H. Zhu, C.C. Lin, W. Luo, S. Shu, Z. Liu, Y. Liu, J. Kong, E. Ma, Y. Cao, R.S. Liu, X. Chen, Highly efficient non-rare-earth red emitting phosphor for warm white light-emitting diodes, Nat. Commun. 5 (2014) 4312, https://doi.org/10.1038/ncomms5312.

[3] S. Li, Q. Zhu, D. Tang, X. Liu, G. Ouyang, L. Cao, N. Hirosaki, T. Nishimura, Z. Huang, R.-J. Xie, Al_2O_3–YAG:Ce composite phosphor ceramic: a thermally robust and efficient color converter for solid state laser lighting, J. Mater. Chem. C 4 (37) (2016) 8648–8654, https://doi.org/10.1039/c6tc03215j.

[4] J. Cho, J.H. Park, J.K. Kim, E.F. Schubert, White light-emitting diodes: history, progress, and future, Laser Photon. Rev. 11 (2) (2017), https://doi.org/10.1002/lpor.201600147.

[5] Q.-Q. Zhu, Y. Meng, H. Zhang, S. Li, L. Wang, R.-J. Xie, YAGG:Ce phosphor-in-YAG ceramic: an efficient green color converter suitable for high-power blue laser lighting, ACS Appl. Energy Mater. 2 (8) (2020) 2644–2650, https://doi.org/10.1021/acsaelm.0c00512.

[6] P. Sun, P. Hu, Y. Liu, S. Liu, R. Dong, J. Jiang, H. Jiang, Broadband emissions from $Lu_2Mg_2Al_2Si_2O_{12}:Ce^{3+}$ plate ceramic phosphors enable a high color-rendering index for laser-driven lighting, J. Mater. Chem. C 8 (4) (2020) 1405–1412, https://doi.org/10.1039/c9tc06068e.

[7] S. You, S. Li, P. Zheng, T. Zhou, L. Wang, L. Liu, N. Horisaki, F. Xu, R.-J. Xie, A thermally robust $La_3Si_6N_{11}$:Ce-in-Glass film for high-brightness blue-laser-driven solid state lighting, Laser Photon. Rev. 13 (2) (2019), https://doi.org/10.1002/lpor.201800216.

[8] T. Deng, L. Huang, S. Li, Q. Zhu, L. Wang, T. Takeda, N. Hirosaki, R.J. Xie, Thermally Robust Orange-Red-Emitting Color Converters for Laser-Driven Warm White Light with High Overall Optical Properties, Laser Photonics Rev, 2022, https://doi.org/10.1002/lpor.202100722.

[9] S. You, S. Li, L. Wang, T. Takeda, N. Hirosaki, R.-J. Xie, Ternary solid solution phosphors $Ca_{1-x-y}Li\ Al_{1-x-y}Si_{1+x+y}N_{3-y}O_y:Ce^{3+}$ with enhanced thermal stability for high-power laser lighting, Chem. Eng. J. 404 (2021) 1–7, https://doi.org/10.1016/j.cej.2020.126575.

[10] Q. Yao, P. Hu, P. Sun, M. Liu, R. Dong, K. Chao, Y. Liu, J. Jiang, H. Jiang, YAG:Ce^{3+} transparent ceramic phosphors brighten the next-generation laser-driven lighting, Adv. Mater. 32 (19) (2020), e1907888, https://doi.org/10.1002/adma.201907888.

[11] P. Zheng, S. Li, R. Wei, L. Wang, T.L. Zhou, Y.R. Xu, T. Takeda, N. Hirosaki, R. J. Xie, Unique design strategy for laser-driven color converters enabling superhigh-luminance and high-directionality white light, Laser Photon. Rev. 13 (10) (2019), https://doi.org/10.1002/lpor.201900147.

[12] Y. Peng, J. Liu, Y. Mou, M. Chen, X. Luo, Heat dissipation enhancement of phosphor-converted white laser diodes by thermally self-managing phosphor-in-glass, IEEE Trans. Electron. Dev. 67 (10) (2020) 4288–4292, https://doi.org/10.1109/ted.2020.3017151.

[13] V.V. Atuchin, N.F. Beisel, E.N. Galashov, E.M. Mandrik, M.S. Molokeev, A. P. Yelisseyev, A.A. Yusuf, Z. Xia, Pressure-stimulated synthesis and luminescence properties of microcrystalline $(Lu,Y)_3Al_5O_{12}:Ce^{3+}$ garnet phosphors, ACS Appl. Mater. Interfaces 7 (47) (2015) 26235–26243, https://doi.org/10.1021/acsami.5b08411.

[14] H. Ji, L. Wang, M.S. Molokeev, N. Hirosaki, R. Xie, Z. Huang, Z. Xia, O.M. ten Kate, L. Liu, V.V. Atuchin, Structure evolution and photoluminescence of $Lu_3(Al,Mg)_2(Al,Si)_3O_{12}:Ce^{3+}$ phosphors: new yellow-color converters for blue LED-driven solid state lighting, J. Mater. Chem. C 4 (28) (2016) 6855–6863, https://doi.org/10.1039/c6tc00966b.

[15] J. Xu, Y. Yang, Z. Guo, B. Hu, J. Wang, B. Du, B. Liu, H. Ji, C. Dam-Hansen, O. B. Jensen, Design of a $CaAlSiN_3$:Eu/glass composite film: facile synthesis, high saturation-threshold and application in high-power laser lighting, J. Eur. Ceram. Soc. 40 (13) (2020) 4704–4708, https://doi.org/10.1016/j.jeurceramsoc.2020.05.029.

[16] J. Park, J. Kim, H. Kwon, Phosphor-Aluminum composite for energy recycling with high-power white lighting, Adv. Opt. Mater. 5 (19) (2017), https://doi.org/10.1002/adom.201700347.

[17] D. Zhang, W. Xiao, C. Liu, X. Liu, J. Ren, B. Xu, J. Qiu, Highly efficient phosphor-glass composites by pressureless sintering, Nat. Commun. 11 (1) (2020) 2805, https://doi.org/10.1038/s41467-020-16649-z.

[18] J. Xu, Y. Yang, J. Wang, B. Du, A.A. Santamaría, B. Hu, B. Liu, H. Ji, C. Dam-Hansen, O.B. Jensen, Industry-friendly synthesis and high saturation threshold of a LuAG:Ce/glass composite film realizing high-brightness laser lighting, J. Eur. Ceram. Soc. 40 (15) (2020) 6031–6036, https://doi.org/10.1016/j.jeurceramsoc.2020.06.074.

[19] S. Hu, C. Lu, G. Zhou, X. Liu, X. Qin, G. liu, S. Wang, Z. Xu, Transparent YAG:Ce ceramics for WLEDs with high CRI: Ce^{3+} concentration and sample thickness effects, Ceram. Int. 42 (6) (2016) 6935–6941, https://doi.org/10.1016/j.ceramint.2016.01.079.

[20] Y. Gao, J. Qiu, D. Zhou, Investigation of optical properties: Eu with Al codoping in aluminum silicate glasses and glass-ceramics, J. Am. Ceram. Soc. 100 (7) (2017) 2901–2913, https://doi.org/10.1111/jace.14807.

[21] Y.H. Nam, K. Han, W.J. Chung, W.B. Im, Color conversion properties of various thick-film phosphor-in-glasses depending on structural design for white LEDs, J. Am. Ceram. Soc. 103 (8) (2020) 4266–4274, https://doi.org/10.1111/jace.17123.

[22] R. Wei, L. Wang, P. Zheng, H. Zeng, G. Pan, H. Zhang, P. Liang, T. Zhou, R. Xie, On the luminance saturation of phosphor-in-glass (PiG) films for blue-laser-driven white lighting: effects of the phosphor content and the film thickness, J. Eur. Ceram. Soc. 39 (5) (2019) 1909–1917, https://doi.org/10.1016/j.jeurceramsoc.2019.01.024.

[23] H. Yang, Y. Zhang, Y. Zhang, Y. Zhao, X. Liang, G. Chen, Y. Liu, W. Xiang, Designed glass frames full color in white light-emitting diodes and laser diodes lighting, Chem. Eng. J. 414 (2021), https://doi.org/10.1016/j.cej.2021.128754.

[24] L. Wang, H. Yang, Y. Zhang, Y. Liang, J. Zhang, E. Mei, F. Xu, J. Long, P. Yu, W. Xiang, All-inorganic high efficiency LuAG:Ce^{3+} converter based on phosphor-in-glass for laser diode lighting, J. Alloys Compd. 892 (2022), https://doi.org/10.1016/j.jallcom.2021.161882.

[25] J. Zhang, H. Yang, Y. Zhang, X. Liu, Y. Zhang, Y. Liang, H. Li, B. Ma, X. Liang, W. Xiang, Stable phosphor-in-glass realizing ultrahigh luminescence efficiency for high-power laser-driven lighting, Appl. Phys. Lett. 119 (2) (2021), https://doi.org/10.1063/5.0055656.

[26] Y.-F. Huang, Y.-C. Chi, C.-H. Cheng, C.-T. Tsai, W.-C. Wang, D.-W. Huang, L.-Y. Chen, G.-R. Lin, LuAG:Ce/CASN:Eu phosphor enhanced high-CRI R/G/B LD lighting fidelity, J. Mater. Chem. C 7 (31) (2019) 9556–9563, https://doi.org/10.1039/c9tc01586h.

[27] P. Huang, Y. Zhao, J. Wang, Y. Zheng, P. Yang, Q. Zheng, S. Gu, B. Zhou, W. Jiang, L. Wang, Tunable chromaticity and high color rendering index of WLEDs with $CaAlSiN_3:Eu^{2+}$ and YAG:Ce^{3+} dual phosphor-in-silica-glass, J. Am. Ceram. Soc. 103 (9) (2020) 4989–4998, https://doi.org/10.1111/jace.17210.

[28] R. Xiang, X. Liang, P. Li, X. Di, W. Xiang, A thermally stable warm WLED obtained by screen-printing a red phosphor layer on the LuAG:Ce^{3+} PiG substrate, Chem. Eng. J. 306 (2016) 858–865, https://doi.org/10.1016/j.cej.2016.08.008.

[29] Z. Liu, P. Hu, H. Jiang, P. Sun, Y. Liu, Z. Luo, J. Xu, Z. Huang, J. Jiang, $CaAlSiN_3:Eu^{2+}/Lu_3Al_5O_{12}:Ce^{3+}$ phosphor-in-glass film with high luminous efficiency and CRI for laser diode lighting, J. Mater. Chem. C 9 (10) (2021) 3522–3530, https://doi.org/10.1039/d1tc00136a.

[30] Y. Zhang, Y. Liang, Y. Zhang, X. Liu, Y. Yu, Y. Zhao, X. Liang, W. Xiang, High color rendering index composite phosphor-in-glass for high-power white laser lighting, J. Eur. Ceram. Soc. 41 (9) (2021) 4915–4923, https://doi.org/10.1016/j.jeurceramsoc.2021.03.040.

[31] Q. Huang, P. Sui, F. Huang, H. Lin, B. Wang, S. Lin, P. Wang, J. Xu, Y. Cheng, Y. Wang, Toward High-Quality Laser-Driven Lightings: Chromaticity-Tunable Phosphor-in-Glass Film with "Phosphor Pattern" Design, Laser Photonics Rev, 2022, https://doi.org/10.1002/lpor.202200040.

[32] Y. Peng, R. Li, H. Cheng, Z. Chen, H. Li, M. Chen, Facile preparation of patterned phosphor-in-glass with excellent luminous properties through screen-printing for high-power white light-emitting diodes, J. Alloys Compd. 693 (2017) 279–284, https://doi.org/10.1016/j.jallcom.2016.09.197.

[33] H. Lin, T. Hu, Y. Cheng, M. Chen, Y. Wang, Glass ceramic phosphors: towards long-lifetime high-power white light-emitting-diode applications-A review, Laser Photon. Rev. 12 (6) (2018), https://doi.org/10.1002/lpor.201700344.

[34] R. Zhang, H. Lin, Y. Yu, D. Chen, J. Xu, Y. Wang, A new-generation color converter for high-power white LED: transparent Ce^{3+}:YAG phosphor-in-glass, Laser Photon. Rev. 8 (1) (2014) 158–164, https://doi.org/10.1002/lpor.201300140.

[35] R. Xiang, X. Liang, Q. Xi, Z. Yuan, C. Chen, W. Xiang, A chromaticity-tunable white LED by screen-printing red phosphor coating on PiG plates, Ceram. Int. 42 (16) (2016) 19276–19282, https://doi.org/10.1016/j.ceramint.2016.09.094.

[36] A. Arellano-Morales, J. Molina-González, H. Desirena, J.M. Bujdud-Perez, S. Calixto, High CRI in phosphor-in-doped glass under near-ultraviolet excitation for warm white light-emitting diode, J. Lumin. 229 (2021), https://doi.org/10.1016/j.jlumin.2020.117684.

[37] D. Han, D.S. Li, Y.J. Zhang, H. Lin, E.Y.B. Pun, Crystalline-phase depuration in Ce^{3+} activated $Lu_3Al_5O_{12}$-tellurite green-emitting phosphor-in-glass, J. Lumin. 214 (2019), https://doi.org/10.1016/j.jlumin.2019.116531.

[38] Y. Zhang, Z. Zhang, X. Liu, G. Shao, L. Shen, J. Liu, W. Xiang, X. Liang, A high quantum efficiency $CaAlSiN_3:Eu^{2+}$ phosphor-in-glass with excellent optical

performance for white light-emitting diodes and blue laser diodes, Chem. Eng. J. 401 (2020), https://doi.org/10.1016/j.cej.2020.125983.

[39] J. Xu, Y. Yang, Z. Jiang, B. Hu, X. Wang, H. Ji, J. Wang, Z. Guo, B. Du, C. Dam-Hansen, O.B. Jensen, $CaAlSiN_3$:Eu/glass composite film in reflective configuration: a thermally robust and efficient red-emitting color converter with high saturation threshold for high-power high color rendering laser lighting, Ceram. Int. 47 (11) (2021) 15307–15312, https://doi.org/10.1016/j.ceramint.2021.02.094.

[40] H. Ding, Z. Liu, P. Hu, Y. Liu, P. Sun, Z. Luo, X. Chen, H. Jiang, J. Jiang, High efficiency green-emitting LuAG:Ce ceramic phosphors for laser diode lighting, Adv. Opt. Mater. 2002141 (2021), https://doi.org/10.1002/adom.202002141.